International Journal of Electrical Engineering and Technology (IJEET)
Volume 11, Issue 7, September 2020, pp. 122-141, Article ID: IJEET_11_07_012
Available online at https://iaeme.com/Home/issue/IJEET?Volume=11&Issue=7
ISSN Print: 0976-6545 and ISSN Online: 0976-6553
DOI: https://doi.org/10.34218/IJEET_11_07_012

DIVERSE DYNAMICAL PATTERNS IN A COMPLEX DIGITAL NETWORK OF DELAYED ENGINEERING SYSTEM OF PHASE-LOCKED LOOPS

Bishwajit Paul*
*Department of Physics, Krishnagar Government College,
Krishnagar-741 101, West Bengal, India.

***Corresponding Author**: Bishwajit Paul
*Email: paulbishwajit10@gmail.com

ABSTRACT

Studies on complex networks with engineering systems have significant challenges for researchers. In this article, we demonstrate diverse intricate dynamical patterns in a one dimensional network of diffusivity coupled time-delayed digital phase-locked loops. Systems that utilize time-delayed feedback control are crucial in numerous engineering applications. In modern complex networks, time delayed systems increase the stability of the systems. Recently, many complex nonlinear networks are studied in different litterateurs, such as, complex computer networks, electrical grid systems, FPGA systems and many model neuronal networks. The dynamics of such networks exhibit extremely complex nonlinear phenomena. Therefore, it is very challenging to work with these in reality. To demonstrate such complex network we consider an one dimensional network of locally coupled time-delay feedback controlled digital-phase locked loop (TDFC-DPLL). TDFC-DPLL is more advanced version of DPLL compared to conventional DPLL. It has wider lock range, small steady state phase error and very

less convergence time compared to ordinary single-sampler based positive zero-crossing DPLL (ZC1-DPLL). In a network of one dimensional array it shows several spatiotemporal patterns. Some of the important distinct patterns are synchronized fixed point (SFP), frozen random pattern (FRP), pattern selection (PS), travelling random pattern (TRP), spatiotemporal intermittency (STI), spatiotemporal chaos and chimera state. All those dynamical patterns are drawn on a phase diagram to grab the total dynamics. We derived the stability condition of the network for stable phase-locked operation. A comprehensive analysis of travelling random pattern is presented. This investigation explores the emergence of chimera states (in local coupled system) that occur predominantly in areas with very low coupling strength and higher nonlinearty parameter values. Additionally, the pathway of dynamic phase transition via the chimera state is demonstrated.

Keywords: Complex networks, conversational digital phase-locked loop (DPLL), time-delay feedback controlled digital phase-locked loop (TDFC-DPLL), stability analysis, chimera state, travelling random pattern

Cite this Article: Bishwajit Paul. Diverse dynamical patterns in a complex digital network of delayed engineering system of phase-locked loops. *International Journal of Electrical Engineering and Technology (IJEET)*, 11(7), 2020, pp. 122-141.

https://iaeme.com/Home/issue/IJEET?Volume=11&Issue=7

1. Introduction

In engineering systems, the most complex network arise in internet, power grid systems, communication technology, IC technology, and FPGA systems. In the biological systems, complex networks appears in the human brain and the nervous system of animals. But, such network co-ordinates all the actions and transmit signals throughout the body. As neurons are nonlinear systems, therefore it is impossible to construct such a huge model network in laboratory for experimental realization of the network dynamics with the help of actual neurons. On the other hand, we use huge network in internet and complex computer systems. Therefore, it is very useful and easy to construct model complex networks with the help of electronic or engineering nonlinear systems. So, here we employ digital phase-locked loops (DPLLs) to construct a complex network model.

DPLLs have immense applications in electronic-communication systems and in control systems. In such systems phase locking and frequency matching are of most important criteria.

To achieve these, wide variety of phase-locked loops (PLLs) have invented. For example, uniform sampling DPLL [1], positive zero-crossing DPLL (ZC1-DPLL) [2-5], dual-sampler based zero-crossing DPLL (ZC2-DPLL) [6], time-delayed digital tan-lock loop (TDTL) [7], bang bang DPLL [8] just to name a few. All these are nonlinear feedback controlled systems that show bifurcation and chaos. Among these ZC1-DPLL is widely used in most of the engineering systems due to its circuit simplicity and reliability. Recently, the dynamics of ZC1-DPLL is improvement by the application of time-delayed feedback control (TDFC) technique [9]. TDFC algorithm can improve some basic and important requisites of DPLLs; namely, wider lock range, less steady state phase error and higher speed of convergence towards phase synchronization. This improved version of ZC1-DPLL is called time-delayed feedback controlled digital phase-locked Loop (TDFC-DPLL). So it is desirable in all applications to replace the conventional ZC1-DPLLs by their improved version (TDFC-DPLL). Above merits of TDFC-DPLL is attractive to engineers to make their system much faster in response and reliable in all applications.

The applications of DPLLs, now a day, are not restricted to isolated systems like motor speed control, coherent phase detection, frequency modulation, frequency synthesis, etc. Instead they are widely used in networks, e.g., in synchronous communication, networking, FPGA systems etc. So it is important to study the collective dynamics of DPLLs. Previously the collective dynamics of ZC1-DPLL is studied under local [10] and non-local coupling [11]. But the collective dynamics of TDFC-DPLLs is yet unexplored. In this view, one dimensional network of TDFC-DPLLs is constructed with local coupling and periodic boundary conditions. This paper explores the detail dynamical behavior of such physically realizable engineering network.

Firstly, the system equation of the network is formulated and the local stability analysis is carried out on the basis of fixed point theorem. Several distinct spatiotemporal patterns are identified by the numerical simulation; e.g., synchronized fixed point (SFP), frozen random pattern (FRP), travelling random pattern (TRP), pattern selection (PS), chimera state (CS), spatiotemporal intermittency (STI) and spatiotemporal chaos (STC). A phase diagram is mapped with several colors corresponding to different dynamical patterns. Some representative diagrams of spatiotemporal patterns are depicted to explore the network dynamics. It is identified that, the phase slip direction of TRP changes randomly with system parameters. Phase velocities of TRP are calculated for different parameter values and investigated its dependence on the non-linearity parameter and the coupling strength.

The interesting observation is that, this network with local coupling exhibits chimera state in a small parametric region of the phase diagram. Chimera state is characterized by the coexistence of spatial synchronous and de-synchronous oscillation in a network of identical oscillators [12,13]. Chimera states are very common with nonlocal coupling; though they are also reported in several systems with local [14,15] and global coupling [16,17]. Such states in neuro-biological systems can correlate several phenomena like: uni-hemispheric slow-wave sleep for some aquatic mammals and migratory birds [18,19]; human brain disorders, like, epilepsy and Alzheimer's disease [20]. Chimera states are observed in variety of non-biological laboratory systems, like, chemical oscillators [21,22], mechanical oscillators [23,24], optical systems [25,26], electronic oscillators [27,28] etc. Exploration of chimera state in real engineering networks are also interesting. Though such states are not desirable for faithful operation of the networks. Yet, it is required to identify the regions where the chimera states appear in the parameter space. This helps one to discard those parameter values for reliable network operation. In the network of TDFC-DPLLs dynamical phase transition through chimera state is depicted. Also, synchronous and de-synchronous regions in the network are discriminated by measuring the local curvature.

The organization of the paper is as follows: firstly, the system description along with the stability analysis of an isolated TDFC-DPLL is presented. Then mathematical formulation of system equation for the network is derived and found local stability criteria for stable phase-locked operation of the network. Numerical results along with the phase diagram are explained. Detail dynamics of TRP is reviled with some measures. In the next, chimera state is explored. Finally, summary of the results are concluded.

2. An isolated TDFC-DPLL: system description:

2.1. Mathematical model of an isolated TDFC-DPLL

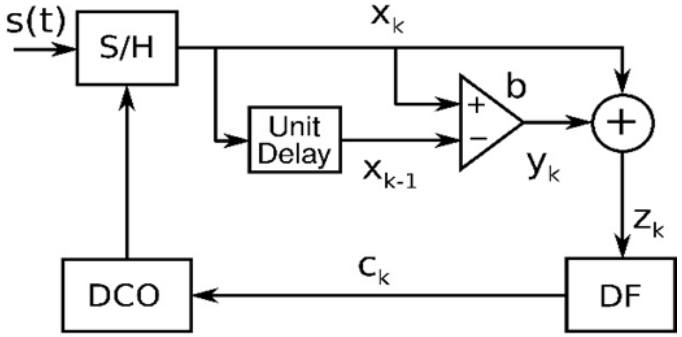

Fig.1 Functional loop diagram of an isolated TDFC-DPLL.

Fig.1 shows the functional loop diagram of a TDFC-DPLL. It comprises of a sample and hold block (S/H), one unit-delay block, a difference amplifier, a digital filter (DF) and a digital controlled oscillator (DCO). Incoming signal $S(t)$ is sampled at its positive zero crossing edges by the S/H block that produces a sequences of sampled signals $\{x_k\}$ corresponding to the time instants t_k . Here, $k \in \{0,1,2,\cdots\}$ represent successive temporal sequence of samplings. The t_k is determined by the DCO controlled by the signal c_k. This c_k is obtained by digital filtering z_k which is the sum of x_k and $y_k = b(x_k - x_{k-1})$. Therefore, $z_k = x_k + b(x_k - x_{k-1})$. Here, b is the gain parameter of the difference amplifier that controls the strength of time-delayed feedback in the loop. In this way, phase locking can be achieved by self-feedback controlling of the DCO frequency.

Consider a noise free sinusoidal incoming signal be $S(t) = asin\,(\omega_t + \theta)$. Where a, ω and θ are respectively the amplitude, angular frequency and initial phase of $S(t)$. If the free-running angular frequency of the DCO be ω_0, then we can write $S(t)$ as

$$S(t) = asin\{\omega_0 t + \psi(t)\} = asin\{\phi(t)\}. \quad (1)$$

Where, $\psi(t) = (\omega - \omega_0)t + \theta$ is the phase angle of $S(t)$ relative to the DCO. From Eq. (1) the sampled signal x_k at t_k may be written as $x_k = S(t_k) = asin(\phi_k)$. Where,

$$\phi_k = \phi(t_k) = \omega_0 t_k + \psi(t_k). \quad (2)$$

The control signal c_k is given by $c_k = G_0 z_k$. Where, G_0 is the gain of the zeroth order DF. The instantaneous time period T_k of the DCO at the k-th sampling instant is logically $T_k = t_k - t_{k-1}$. The algorithm for the next time period of the DCO is given by $T_{k+1} = T_0 - c_k$ [4,29]. Where, $T_0 = 2\,\pi/\omega_0$. Now considering $t_0 = 0$, it is obvious to write the successive sampling instants as,

$$t_k = kT_0 - \sum_{i=0}^{k-1} c_i. \quad (3)$$

From Eq. (2) and (3), phase error at k-th sampling instant becomes,

$$\phi_k = \omega_0\left(kT_0 - \sum_{i=0}^{k-1} c_i\right) + \psi_k. \quad (4)$$

Where, $\psi_k = \psi(t_k)$. The first term $\omega_0 k T_0$ is an integral multiple of 2π. So,

$$\phi_k = \psi_k - \omega_0 \sum_{i=0}^{k-1} c_i. \quad (5)$$

The phase error between two successive sampling instants (t_{k+1} and t_k) becomes,

$$\phi_{k+1} - \phi_k = \psi_{k+1} - \psi_k - \omega_0 G_0 z_k = \Lambda - \xi \omega_0 G_0 z_k. \quad (6)$$

Where, $\xi = \omega/\omega_0$ is the normalized angular frequency of $S(t)$ and $\Lambda = 2\pi(\xi - 1)$ is a constant. Therefore, the phase governing equation of the TDFC-DPLL becomes,

$$\phi_{k+1} = \Lambda + \phi_k - \xi K_1 sin(\phi_k) - b\xi K_1 \{sin(\phi_k) - sin(\phi_{k-1})\}. \quad (7)$$

Where, $K_1 = a\omega_0 G_0$ is called the loop gain of the TDFC-DPLL. All information of $S(t)$ is embedded within ϕ_k which is bounded in $[-\pi: +\pi]$. The Eq. (7) represents the system equation of an isolated TDFC-DPLL [9]. If we set the parameter b at zero, then the system turns into a conventional ZC1-DPLL.

2.2 Stability of an isolated TDFC-DPLL

Stability of the system equation (7) may be found by the method of fixed point theorem. Consider two new variables $\alpha_k = \phi_{k-1}$ and $\beta_k = \phi_k$ such that the Eq. (7) may be expressed as,

$$\alpha_{k+1} = \beta_k, \quad (8a)$$

$$\beta_{k+1} = \Lambda + \beta_k - \xi K_1 sin(\beta_k) - b\xi K_1 \{sin(\beta_k) - sin(\alpha_k)\}. \quad (8b)$$

Therefore the steady state phase error ϕ_s, given by the condition $\beta_{k+1} = \beta_k = \alpha_{k+1} = \alpha_k = \phi_s$, becomes

$$\phi_s = sin^{-1}\left(\frac{\Lambda}{\xi K_1}\right). \quad (9)$$

The Jacobi matrix of the system equations (8) becomes

$$J = \begin{pmatrix} 0 & 1 \\ \xi K_1 b cos(\phi_s) & 1 - \xi K_1 (1+b) cos(\phi_s) \end{pmatrix}. \quad (10)$$

Therefore, the characteristics equation of (10) is given by

$$\lambda^2 + J_1 \lambda + J_2 = 0. \quad (11)$$

Where, $J_1 = -1 + K_1 \xi (1+b) cos(\phi_s)$, $J_2 = -K_1 \xi b cos(\phi_s)$ and λ is the eigenvalue of J. Stability condition can be obtained using Jury's stability criteria as,

$$1 + J_1 + J_2 > 0, \quad (12a)$$

$$1 - J_1 + J_2 > 0, \quad (12b)$$

$$|J_2| < 1. \quad (12c)$$

From the above three inequalities, the conditions of stability become,

$$0 < K_1^2 \xi^2 - \Lambda^2 < \frac{4}{(1+2b)^2}, \quad (13a)$$

$$|b^2 (K_1^2 \xi^2 - \Lambda^2)| < 1. \quad (13b)$$

Fig. 2(a) shows two parameter bifurcation diagram with ξ=1.1. Different colours show different period of oscillations, which are written on the colour pallet. The black regions correspond to higher periodic oscillation or chaos. It is obvious form the figure that, the maximum value of K_1 corresponding to period one oscillation of the system can be obtained by setting feedback control parameter b near the value -0.25. From Eq. (9), the maximum value of K_1 leads to minimum value of steady state phase error. The minimum phase error leads to better phase detection in the system and it is an important criterion for a phase locked loop. Fig 2(b) shows one parameter bifurcation diagram with the corresponding lyapunov spectrum of the isolated system. Practically ξ=1.1 corresponds to a reasonably larger value of frequency offset of the incoming signal S(t) with respect to the DCO.

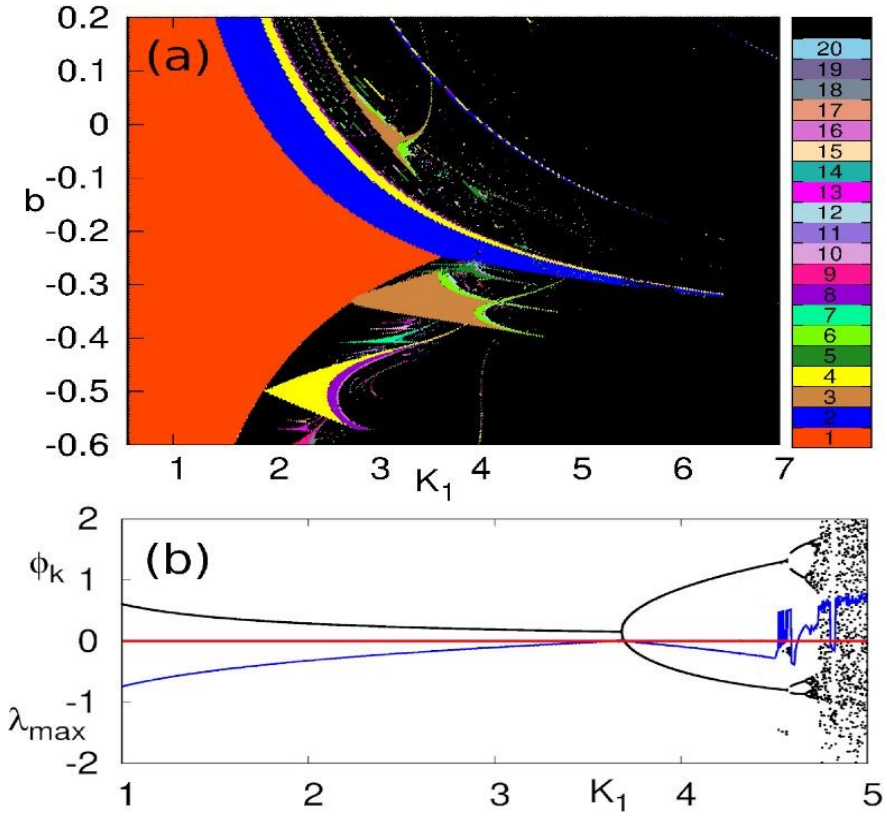

Fig. 2 (a) Shows two parameter bifurcation diagram of an isolated TDFC-DPLL in $(K_1 - b)$ parameter space with $\xi = 1.1$. (b) Shows one parameter bifurcation diagram (black line) along with the maximum values of lyapunov exponents (blue line) for $\xi = 1.1$ and $b = -0.25$. The red line is the reference line corresponding to $\phi_k = 0$ (or, $\lambda_{max} = 0$).

3. One dimensional network of TDFC-DPLLs with local coupling:

3.1 Practical network modeling and formulation of system equation

We construct a one dimensional (1D) network of TDFC-DPLLs with local coupling and periodic boundary condition. The network consists of N identical TDFC-DPLLs as shown in the schematic [Fig. 3(a)]. Each blue solid circle (indexed with $i \in 1,2,3,\cdots,N$) represent TDFC-DPLLs and the nearest neighbour couplings are shown with solid lines. Periodic boundary condition is realized by setting the condition $N + i = i$. Fig. 3(b) shows practical realization of coupling scheme for the i-th TDFC-DPLL which is coupled with the neighbors indexed with $(i-1)$ and $(i+1)$. This coupling is practically implemented by feeding z_k^{i-1} and z_k^{i+1} into the loop by an adder A with adjustable normalized gain parameter $(\epsilon/2)$. Where, ϵ is the strength of coupling. Therefore the signal z_k^i becomes,

$$Z_k^i = x_k^i + b\left(x_k^i - x_{k-1}^i\right) + \frac{\epsilon}{2}\{(1+b)\left(x_k^{i-1} + x_k^{i+1}\right) - b\left(x_{k-1}^{i-1} + x_{k-1}^{i+1}\right)\}. \quad (14)$$

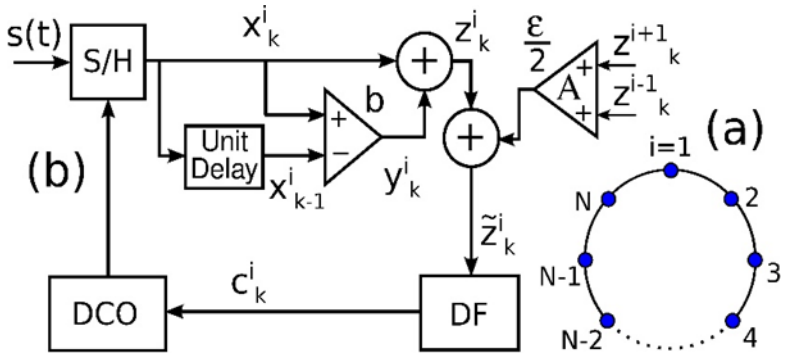

Fig. 3 (a) Network architecture. (b) Functional loop diagram of i-th TDFC-DPLL in the network under local coupling.

Now employing same logic [as in Sec. 2.1], we can arrive at a condition similar to Eq. (6) as

$$\phi_{k+1}^i - \phi_k^i = \Lambda - \xi\omega_0 G_0 Z_k^i. \quad (15)$$

Now using Eq. (14) and Eq. (15), phase error equation is written as

$$\phi_{k+1}^i = \Lambda + \phi_k^i - \xi K_1 sin\left(\phi_k^i\right) - \xi K_1 b\{sin\left(\phi_k^i\right) - sin\left(\phi_{k-1}^i\right)\} - \frac{\epsilon}{2}\xi K_1[(1+ b)\{sin\left(\phi_k^{i-1}\right) + sin\left(\phi_k^{i+1}\right)\} - b\{sin\left(\phi_{k-1}^{i-1}\right) + sin\left(\phi_{k-1}^{i+1}\right)\}]. \quad (16)$$

If we set the parameter b at zero, then the system reduces to an one dimensional network of ZC1-DPLLs with local coupling; the dynamics which has studied earlier in Ref. [10].

3.2 Local stability analysis of the network

The linear stability of a system at the steady state can be derived by diagonalizing the Jacobi matrix of the system. Steady state phase error ϕ_{ss} of the network [Eq. (16)] is given by

$$\phi_{ss} = sin^{-1}\left(\frac{\Lambda}{\xi K_1(1+\epsilon)}\right). \quad (17)$$

The system Eq. (16) can be represented in terms of a $(2N \times 2N)$ Jacobi matrix as,

$$J_{2N} = \begin{pmatrix} 0_N & I_N \\ A_N & B_N \end{pmatrix}. \quad (18)$$

Where 0_N, I_N are respectively the null matrix and identity matrix of order $(N \times N)$ each. A_N, B_N are the circulant matrices of order $(N \times N)$ and has the following form:

$$A_N = \begin{pmatrix} A_d & A_r & 0 & 0 & \cdots & A_l \\ A_l & A_d & A_r & 0 & \cdots & 0 \\ 0 & A_l & A_d & A_r & \cdots & 0 \\ \vdots & \vdots & \vdots & \vdots & \vdots & \vdots \\ A_r & 0 & 0 & \cdots & A_l & A_d \end{pmatrix}, \tag{19}$$

with $A_d = \xi K_1 b cos(\phi_{ss})$, $A_l = A_r = \left(\frac{\epsilon}{2}\right) \xi K_1 b cos(\phi_{ss})$; and

$$B_N = \begin{pmatrix} B_d & B_r & 0 & 0 & \cdots & B_l \\ B_l & B_d & B_r & 0 & \cdots & 0 \\ 0 & B_l & B_d & B_r & \cdots & 0 \\ \vdots & \vdots & \vdots & \vdots & \vdots & \vdots \\ B_r & 0 & 0 & \cdots & B_l & B_d \end{pmatrix}, \tag{20}$$

With $B_d = 1 - \xi K_1 (1 + b) cos(\phi_{ss})$ and $B_l = B_r = -\left(\frac{\epsilon}{2}\right) \xi K_1 (1 + b) cos(\phi_{ss})$. As 0_N and I_N are basically circulant in nature, therefore J_{2N} is a block circulant matrix. A circulant matrix can be diagonalized by a Fourier matrix. The stability condition of Eq. (16) can be evaluated by finding eigenvalues of the matrix J_{2N} and using the criteria: absolute of real parts of all the eigenvalues should be less than one. J_{2N} can be diagonalized by the operation $\frac{1}{N}(D_{2N}^{-1} J_{2N} D_{2N})$ [30]; where D_{2N} and D_{2N}^{-1} are block diagonalizing matrices for a block circulant matrix; they are given by,

$$D_{2N} = \begin{pmatrix} F_N & 0_N \\ 0_N & F_N \end{pmatrix}, \tag{21}$$

and

$$D_{2N}^{-1} = \begin{pmatrix} F_N^{-1} & 0_N \\ 0_N & F_N^{-1} \end{pmatrix}. \tag{22}$$

Here F_N is the Fourier matrix of order (N$\times N$) and F_N^{-1} is the inverse of F_N. Therefore diagonalized matrix of J_{2N} becomes,

$$U_{2N} = \frac{1}{N}(D_{2N}^{-1} J_{2N} D_{2N}) = \begin{pmatrix} 0_N & I_N \\ A_N & B_N \end{pmatrix}. \tag{23}$$

Obviously 0_N and I_N remains invariant under this transformation. Also $\mathcal{A}_N = \frac{1}{N}(F_N^{-1}A_N F_N)$ and $\mathcal{B}_N = \frac{1}{N}(F_N^{-1}B_N F_N)$ become diagonal matrix. Proper similarity transformation can express U_{2N} as a block diagonal matrix, containing N blocks of (2×2) matrices each; i.e.,

$$U_{2N} = \begin{pmatrix} L_1 & 0 & \cdots & 0 \\ 0 & L_2 & \cdots & 0 \\ \vdots & \vdots & \ddots & \vdots \\ 0 & 0 & \cdots & L_N \end{pmatrix}. \tag{24}$$

Where all diagonal blocks are written as,

$$L_l = \begin{pmatrix} 0 & 1 \\ \mathcal{A}_N(l,l) & \mathcal{B}_N(l,l) \end{pmatrix}; \qquad \forall l \in (1,2,3,\cdots,N). \tag{25}$$

Where,

$$\mathcal{A}_N(l,l) = \xi K_1 b cos(\phi_{ss}) + \epsilon \xi K_1 b cos(\phi_{ss}) cos\left(\frac{2\pi(l-1)}{N}\right), \tag{26}$$

and

$$\mathcal{B}_N(l,l) = 1 - \xi K_1(1+b)cos(\phi_{ss}) - \epsilon \xi K_1(1+b)cos(\phi_{ss})cos\left(\frac{2\pi(l-1)}{N}\right). \tag{27}$$

Now for each diagonal block, we can write two eigenvalues as,

$$\lambda_l = \frac{\mathcal{B}_N(l,l) \pm \sqrt{\{\mathcal{B}_N(l,l)\}^2 + 4\mathcal{A}_N(l,l)}}{2}; \qquad \forall l \in (1,2,3,\cdots,N). \tag{28}$$

Hence $2N$ numbers of eigenvalues can be obtained; positive sign in Eq. (28) leads λ_l to $(\lambda_1'\lambda_2', \lambda_3' \ldots)$, while negative sign leads $\lambda_l$to $\left(\bar{\lambda_1}\bar{\lambda_2}, \bar{\lambda_3} \ldots\right)$. Now for stable synchronized solution of the network, real parts of all eigenvalues should be less than unity, i.e.,$|Re(\lambda_l')|_{max}$ and also $\left|Re\left(\bar{\lambda_l}\right)\right|_{max}$ for all $l \in (1,2,\cdots,N)$. In other word it can be written simply as,

$$|Re(\lambda_l)|_{max} < 1. \tag{29}$$

Therefore, equations (29) and (28) together with equations (26), (27) and (17) determine the stability criteria for stable phase-locked condition in 1D network of TDFC-DPLLs. This local stability criterion is the necessary condition for stabilization of the network; but for sufficient condition one has to determine global stability condition. For a complex network of large dimension analytical finding of global stability criteria is very difficult and not traceable [31,32].

4. Numerical results

Numerical simulation on the system Eq. (16) explores several spatiotemporal patterns and chimera state. Throughout the simulation, network length is considered to be $N = 256$ and used random initial condition bounded uniformly within the natural interval $[-\pi: +\pi]$. The periodic boundary condition is realized by setting $\phi_k^{i+N} = \phi_k^i$. The frequency step input to each TDFC-DPLLs are restricted with $\xi = 1.1$ practically such a large value provides sufficiently wide frequency offset to the incoming signal. The parameter b is kept constant at $b = -0.25$ for all the TDFC-DPLLs in the network. For such value of b, each isolated TDFC-DPLLs are very close to their largest possible loop gain $K_1 \approx 3.6$ up to which systems show stable loop operation [9]. Larger values of K_1 leads to the lesser steady state phase error in the network [see Eq. (17)]. Technically, lesser steady states are more desired in the practical applications; because they correspond to better synchronization in the network. Throughout the simulation first 50000 iterations are discarded to eliminate transients.

4.1 Phase diagram

Simulation reveals several important spatiotemporal patterns in the network of TDFC-DPLLs. All the distinct patterns are mapped in a phase diagram shown in Fig. 4(a). Distinct colors, in the $K_1 - \epsilon$ parameter space, corresponds to different spatiotemporal dynamics. For an illustration purpose some of the dynamical patterns are shown in the insets [Fig. 4(b)-(f)]. Also, one route of dynamical phase transition in the network is demonstrated with the increase of $K_1$for a fixed coupling strength ϵ. For this, keeping $\epsilon = 0.1$, K_1 is increased gradually. It is found that the network exhibits following route of dynamical states: synchronized fixed point (SFP), travelling random pattern (TRP), frozen random pattern (FRP), spatiotemporal intermittency (STI), spatiotemporal chaos (STC) and chimera state (CS). Some of these spatiotemporal patterns are shown in the insets [Fig. 4(b)-(f)]. Detail studies on TRP and CS are given in the next subsections. The black dotted line on Fig. 4(a) represents the marginal zone for stable phase-locked operation. The line is found from the stability criteria [Eq. (28)} and (29)]. It confirms complete agreement of analytical result with the numerical outcome. It is noteworthy that, the region of SFP is wider with respect to K_1 compared to that of in the network of conventional ZC1-DPLLs studied in Ref. [10]. Such wider lock range provides lesser phase error in SFP, hence better synchronization in the network.

Let's explore the dynamical phase transition with increase in K_1 for $\epsilon = 0.1$. In Fig. 4(a), the region of SFP is shown with dark green colour. In this dynamics, starting from random initial values, all the TDFC-DPLLs attain a common phase state [given by Eq. (17)] that do not

change in the subsequent temporal sequences. Such spatiotemporal synchronized state has immense practical applications in engineering, communication electronics, clock synchronization etc. Fig. 4(b) shows the state of spatiotemporal synchronization (SFP) of the network in $(i-k)$ plot with colour map. As K_1 is increased beyond a critical value ($K_1 \approx 3.23$) for $\epsilon = 0.1$, the coupling strength fails to maintain synchronization in the network. The system exhibits spatial bifurcation and the whole network is sub-divided into several domains of random size and position as shown in Fig. 4(c). Relative positions of the domains largely depend on initial conditions. But the average widths of the domains decrease with the increase of K_1. We have identified two variants of such pattern dynamics depending on the mobility of the domain boundaries. The domain boundaries may or may not be stationary. If the domains are stationary as shown in Fig. 4(c), such dynamical patterns are called FRP. But if the domains travel in time along the network, then it is called TRP [spatiotemporal dynamics looks like Fig. 5]. For lower values of ϵ, FRP follows the TRP; but for larger values of ϵ, only TRP appears. Detail dynamics of TRP is presented in the next subsection. For further increase in K_1 for fixed $\epsilon = 0.1$, the system shows STI [Fig. 4(e)] which is a mixture of regular and irregular dynamics. Some of the TDFC-DPLLs may oscillate periodically for an interval, but they meanwhile may become independently chaotic. With the increase in K_1 more, the system becomes completely chaotic spatially as well as temporally. Such dynamics is called STC [Fig. 4(f)]. Thereafter, for even larger values of K_1, chimera states appears for a small parametric region.

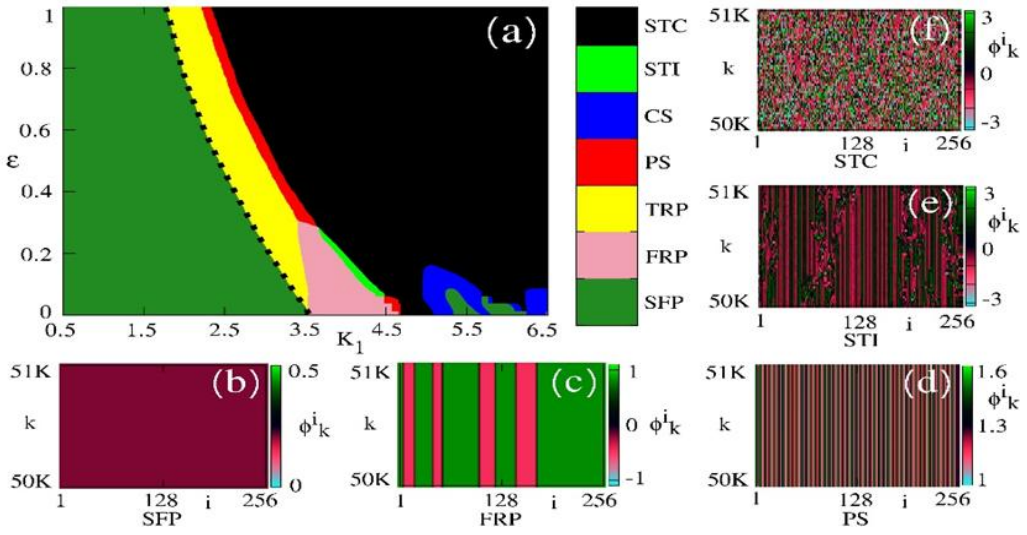

Fig. 4 (a) Phase diagram in $K_1 - \epsilon$ parameter space for $\xi = 1.1$, $b = -0.25$; (b) SFP: $\epsilon = 0.1$, $K_1 = 2.5$; (c) FRP: $\epsilon = 0.1$, $K_1 = 3.6$; (d) PS: $\epsilon = 0.45$, $K_1 = 3.15$; (e) STI: $\epsilon = 0.1$, $K_1 = 4.238$; (f) STC: $\epsilon = 0.1$, $K_1 = 5.7$.

The major part of PS in the phase diagram appears after the TRP for larger values of ϵ. The dynamics of PS is shown in Fig. 4(d). Here the network is subdivided into small but nearly equal width domains. The domain widths are independent of the initial conditions, but depend on parameter values. For smaller values of ϵ and larger values of K_1, there appear horse shore shaped blue island in the phase diagram, where the network exhibit CS. The dynamics of CS is explained in the next.

4.2 Travelling random pattern

Like FRP, domains of TRP are random in size and position. But unlike FRP, the domains of TRP move in time along the network. The cause of movement of the domains is the phase slip in successive temporal sequences. It is observed that, for same initial conditions, the direction of travel randomly change with K_1 and ϵ. To illustrate this, keeping ϵ constant at 0.40, K_1 is increased in small steps and observed the direction of propagation of the domains of TRP. Fig. 5(a1)-(b1) show TRP pattern for the parameters $K_1 = 3.16$ and $\epsilon = 0.4$. Here the domain boundaries move towards right, i.e., along the increasing values of i. While slight increase in K_1, reverses the direction of propagation (i.e., along the decreasing values of i). This is shown in Fig. 5(a2)-(b2) [$K_1 = 3.18$, $\epsilon = 0.4$]. While it changes again into the right side for slight change in K_1 as shown in Fig. 5(a3)-(b3) [$K_1 = 3.2$, $\epsilon = 0.4$]. It is also noteworthy from these figures that the sizes, positions and the number of domains change arbitrarily with the change of K_1. This is also true for the change in ϵ keeping K_1 constant. It is also found that not only the direction of phase slip, but also the rate of phase slip change with the parameters K_1 and ϵ. But the rate of phase slip is not random with the change of parameters; instead it follows some definite rule. Next we explore the rule that govern the rate of phase slip.

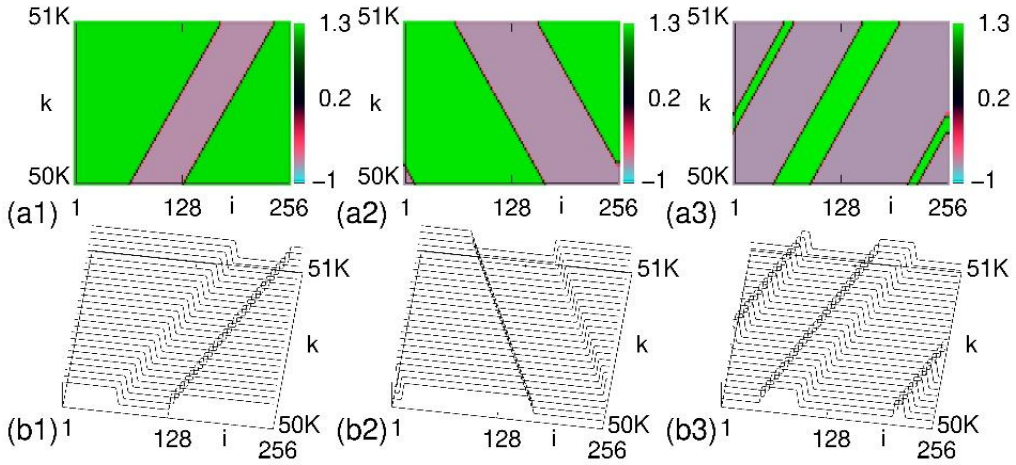

Fig. 5 TRP: $\xi = 1.1$, $b = -0.25$ and $\epsilon = 0.4$. Shows the random change in directions of propagation with the change of K_1. (a1)-(a3) are the space-time plot of ϕ_k^i with colors, whereas (b1)-(b3) are the same plot with lines. (a1)-(b1) $K_1 = 3.16$; (a2)-(b2) $K_1 = 3.18$; (a3)-(b3) $K_1 = 3.20$.

The rate of phase slip, called the phase velocity(V_p), is defined as the shift of domain boundaries along the site indices of the network per unit time. Geometrically it is determined by $V_p = \frac{\Delta i}{\Delta k}$, as shown in the Fig. 6(a). Where, Δi is the shift of the domain boundaries in the time interval Δk. So, it is measured by the inclination of the trajectories of domain boundaries in spatiotemporal $(i - k)$ plots. Now if the domain boundaries shift towards right then we may call V_p to be positive otherwise it is negative. Fig. 6(a) [$K_1 = 3.0$, $\epsilon = 0.26$] and 6(b) [$K_1 = 2.5$, $\epsilon = 0.80$] show the different TRP velocities for different parameter values; because the inclinations of the colour strips [domain boundaries] with the space axis i are different in two plots. To realize the parameter dependence of V_p on K_1 and ϵ, we plot two graphs. The Fig. 6(c) shows the variation of $|V_p|$ with K_1 for constant values of ϵ and the Fig. 6(d) explores the dependence of $|V_p|$ on ϵ for constant values of K_1. It is obvious from Fig. 6(c) that, for larger values of ϵ, $|V_p|$ increases almost linearly with K_1; but for smaller values of ϵ, $|V_p|$ changes according to cubic polynomial in K_1. The polynomial that fits best with the experimental data can be written as $|V_p| = c_3 K_1^3 + c_2 K_1^2 + c_1 K_1 + c_0$, where the coefficients (c_3, c_2, c_1, c_0) for different $\epsilon$are given in the Table 1. It is obvious that absolute values of the coefficients increases with the decrease in ϵ. Fig. 6(d) shows that, $|V_p|$ increases almost linearly with ϵ when K_1 is kept fixed.

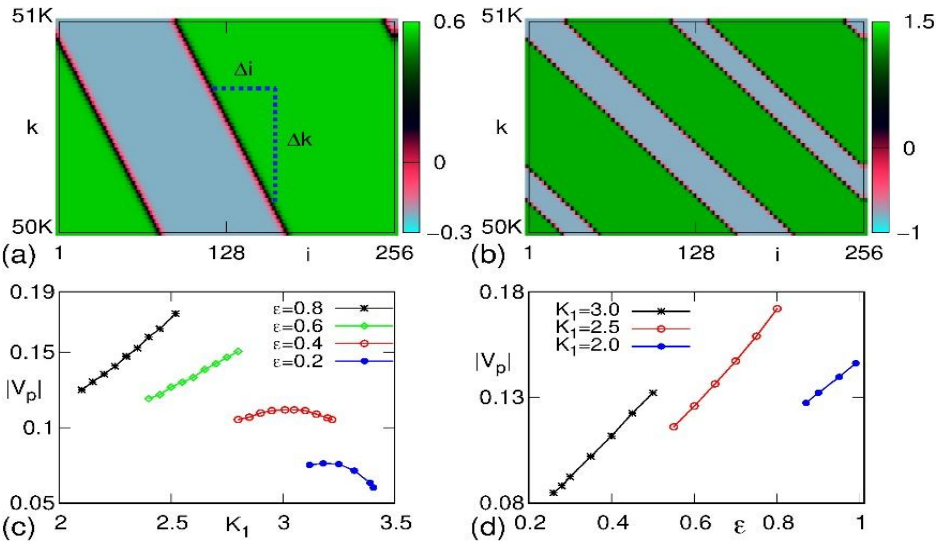

Fig. 6 Phase velocity of TRP: constant parameters $\xi = 1.1$, $b = -0.25$. (a) TRP for $K_1 = 3.0$ and $\epsilon = 0.26$. (b) TRP for $K_1 = 2.5$ and $\epsilon = 0.80$. The inclination of the domain boundaries with i-axis in (b) is greater than that of in (a). (c) Variation of $|V_p|$ on K_1 for fixed values of ϵ . (d) Dependence of $|V_p|$ on ϵ for constant values of K_1.

Table 1 Coefficients of cubic polynomial that fit best with the experimental data plotted in Fig. 6(c)

ϵ	c_3	c_2	c_1	c_0
0.8	-0.0280863	0.242712	-0.550632	0.471218
0.6	-0.112175	0.894337	-2.29279	2.02119
0.4	-0.123481	0.962226	-2.43076	2.078
0.2	-0.638219	5.88256	-18.0432	18.4904

4.3 Chimera state

The network of TDFC-DPLLs with local coupling exhibits chimera state within small islands surrounded by chaotic region as shown in the parameter space. Chimera state embedded within the chaotic region is rarer in the other networks. To explore the chimera state and the transition route surrounding the chimera state, coupling parameter is kept constant at $\epsilon = 0.1$ and K_1 is increased gradually in small steps. Fig. 7 depicts the phase transition route: $STC \rightarrow CS \rightarrow SFP$. Spatial variation of phases are shown in Fig. 7(a1), (b1) and (c1) corresponding to STC, CS, and SFP respectively. Fig. 7(a1) shows STC for $\epsilon = 0.1$ and $K_1 = 5.05$. The dynamics changes to chimera state for small increase in K_1 [Fig. 7(b1): $\epsilon = 0.1$ and $K_1 = 5.13$].

It shows the coexistence of synchronous and asynchronous zones of TDFC-DPLLs in the network. It is observed that for small increase in $K_1$the network becomes synchronized [Fig. 7(c1): $\epsilon = 0.1$ and $K_1 = 5.25$] and the system enters into the very small synchronized zone embedded within the chimera state as shown in the phase diagram. This SFP region is independent of initial conditions.

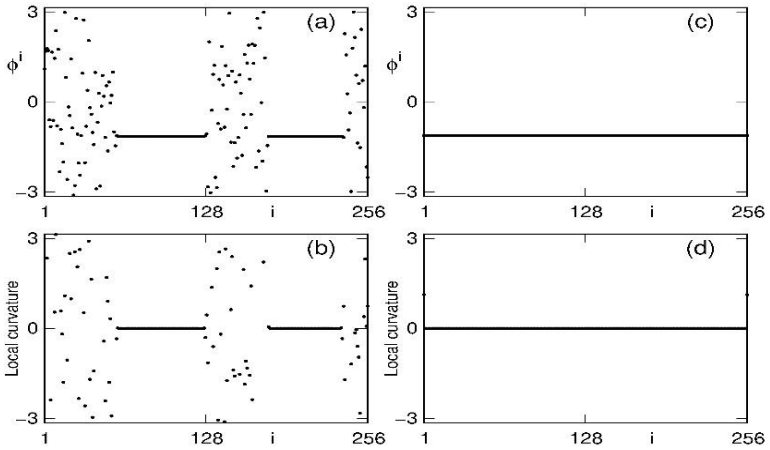

Fig. 7 Phase transition from $STC \rightarrow CS \rightarrow SFP$, $\xi = 1.1$, $b = -0.25$, $\epsilon = 0.1$; (a1)-(a2) STC: $K_1 = 5.05$; (b1)-(b2) CS: $K_1 = 5.13$; (c1)-(c2) SFP: $K_1 = 5.25$.

To discriminate among the spatial coherence and incoherence in the chimera state we use the concept of local curvature recently proposed by Kemath et. al. [33]. It is defined by the second order derivative of local phase states with respect to spatial indices of each TDFC-DPLLs in the network. Mathematically, it is written as,

$$D_k^i = \nabla\left(\nabla\phi_k^i\right) = \nabla\phi_k^i - \nabla\phi_k^{i-1} = \left(\phi_k^{i+1} - \phi_k^i\right) - \left(\phi_k^i - \phi_k^{i-1}\right) = \phi_k^{i+1} - 2\phi_k^i + \phi_k^{i-1} \qquad (30)$$

Local curvature D_k^i for STC, CS and SFP are shown in the Fig. 7(a2), (b2) and (c2) respectively. It is obvious that local curvature for the synchronous regions becomes zero and it fluctuates randomly in the asynchronous regions. Therefore, local curvature is a good identifier for the chimera state.

5 Conclusion:

In this paper we have studied the complex dynamical patterns in a network of TDFC-DPLLs. Several distinct spatiotemporal dynamical patterns have identified including spatiotemporal

chaos. All these patterns are mapped on a phase diagram. Also, the region of stable fixed point has been derived analytically using linear stability analysis. In real network systems, SFP is the requisite state of reliable network operation. Therefore, the region of the stable fixed point in the phase diagram can guide engineers to choose the parameter values in constructing a network of TDFC-DPLLs. In compression to the network of conventional ZC1-DPLLs, this network exhibits wider lock range corresponding to K_1; this leads to lesser steady state phase error and hence better synchronization in the network. This engineering network can be constructed with the help of FPGA system and may be used to demonstrate chimera state experimentally in electronic systems. We belief that, the TRP can be used for transmission of special signals in the engineering networks.

REFERENCES

[1] M. Zoltowski (2001) Some advances and refinements in digital phase locked loops (DPLLs) Signal Processing 81 735-789.

[2] G.M. Bernstein, M.A. Liberman, A.J. Lichtenberg (1989) Nonlinear dynamics of a digital phase locked loop Communications, IEEE Transactions 37 10 1062-1070.

[3] G. A. Leonov, S. M. Seledzhi (2005) Stability and bifurcations of phase locked loops for digital signal processors Int. J. Bifurcation and Chaos 15 1347-1360.

[4] Tanmoy Banerjee and B.C. Sarkar (2005) Phase error dynamics of a class of modified second-order digital phase-locked loops in the background of cochannel interference Signal Processing 85 8 1611-1622.

[5] T. Banerjee, B. C. Sarkar (2008) Chaos and bifurcation in a third-order digital phase locked loop Int. J. Electron. and Commun. 62 86-91.

[6] T. Banerjee, B. C. Sarkar (2009) Chaos, intermittency and control of bifurcation in a ZC2-DPLL Int. J. Electron. 96 717-732 2009.

[7] Z. M. Hussain, B. Boashash (2002) The time-delay digital tanlock loop: Performance analysis in additive gaussian noise Journal of the Franklin Institute 399 43-60.

[8] N. D. Dalt (2005) A design oriented study of the nonlinear dynamics of a digital bang-bang PLLs IEEE Trans. on Circuit and Syst.-I 52 21-31.

[9] Tanmoy Banerjee, B. C. Sarkar (2012) Conventional and extended time-delayed feedback controlled zero-crossing digital phase locked loop Int. J of Bifurcation and Chaos 22 12 1230044.

[10] Tanmoy Banerjee, Bishwajit Paul, and B. C. Sarkar (2014) Spatiotemporal dynamics of a digital phase-locked loop based coupled map lattice system Chaos: An Interdisciplinary Journal of Nonlinear Science 24 1 013116.

[11] Bishwajit Paul, Tanmoy Banerjee (2019) Chimeras in digital phase-locked loops Chaos: An Interdisciplinary Journal of Nonlinear Science 29 1 013102.

[12] Daniel M. Abrams, Steven H. Strogatz (2004) Chimera states for coupled oscillators Phys. Rev. Lett. 93 174102.

[13] Mark J Panaggio, Daniel M Abrams (2015) Chimera states: coexistence of coherence and incoherence in networks of coupled oscillators Nonlinearity 28 3 R67.

[14] Carlo R. Laing (2015) Chimeras in networks with purely local coupling Phys. Rev. E 92 050904.

[15] Srilena Kundu, Bidesh K. Bera, Dibakar Ghosh, M. Lakshmanan (2019) Chimera patterns in three-dimensional locally coupled systems Phys. Rev. E 99 022204.

[16] Gautam C. Sethia, Abhijit Sen (2014) Chimera states: The existence criteria revisited Phys. Rev. Lett. 112 144101.

[17] Lennart Schmidt, Katharina Krischer (2015) Chimeras in globally coupled oscillatory systems: From ensembles of oscillators to spatially continuous media Chaos: An Interdisciplinary Journal of Nonlinear Science 25 6 064401.

[18] Rattenborg NC, Amlaner CJ, Lima SL (2000) Behavioral, neurophysiological and evolutionary perspectives on unihemispheric sleep Neurosci Biobehav Rev. 24 817-42.

[19] Niels C Rattenborg (2006) Do birds sleep in flight? Naturwissenschaften 93 413-425.

[20] Ralph G. Andrzejak, Christian Rummel, Florian Mormann, Kaspar Schindler (2016) All together now: Analogies between chimera state collapses and epileptic seizures Scientific Reports 6 23000.

[21] Mark R. Tinsley, Simbarashe Nkomo, Kenneth Showalter (2012) Chimera and phase-cluster states in populations of coupled chemical oscillators Nature Physics 8 662-665.

[22] Simbarashe Nkomo, Mark R. Tinsley, Kenneth Showalter (2016) Chimera and chimera-like states in populations of nonlocally coupled homogeneous and heterogeneous chemical oscillators Chaos: An Interdisciplinary Journal of Nonlinear Science 26 9 094826.

[23] T. Bountis, V. G. Kanas, J. Hizanidis, A. Bezerianos (2014) Chimera states in a two–population network of coupled pendulum–like elements The European Physical Journal Special Topics 223 721-728.

[24] Erik Andreas Martens, Shashi Thutupalli, Antoine Fourrière, Oskar Hallatschek (2013) Chimera states in mechanical oscillator networks The Proceedings of the National Academy of Sciences 110 10563-10567.

[25] Fabian Böhm, Anna Zakharova, Eckehard Schöll, Kathy Lüdge (2015) Amplitude-phase coupling drives chimera states in globally coupled laser networks Phys. Rev. E 91 040901.

[26] J Shena, J Hizanidis, V Kovanis, G. P Tsironis (2017) Turbulent chimeras in large semiconductor laser arrays Scientific Reports 7 42116.

[27] Lucia Valentina Gambuzza, Arturo Buscarino, Sergio Chessari, Luigi Fortuna, Riccardo Meucci, Mattia Frasca. (2014) Experimental investigation of chimera states with quiescent and synchronous domains in coupled electronic oscillators Phys. Rev. E 90 032905.

[28] Laurent Larger, Bogdan Penkovsky, Yuri Maistrenko (2013) Virtual chimera states for delayed-feedback systems Phys. Rev. Lett. 111 054103.

[29] W.C. Lindsey, Chak Ming Chie (1981) A Survey of Digital Phase-Locked Loops. In: Proceedings of the IEEE 69 4 410-431.

[30] Prashant M. Gade (1998) Feedback control in coupled map lattices Physical Review E 57 6 7309-7312.

[31] K. Kaneko (1989) Pattern dynamics in spatiotemporal chaos: Pattern selection, diffusion of defect and pattern competition intermettency Physica D: Nonlinear Phenomena 34 1-2 1-41.

[32] K. Kaneko (1993) "Theory and Applications of Coupled Map Lattices". Wiley, Chichester.

[33] Felix P. Kemeth, Sindre W. Haugland, Lennart Schmidt, Ioannis G. Kevrekidis, and Katharina Krischer (2016) A classification scheme for chimera states Chaos: An Interdisciplinary Journal of Nonlinear Science 26 094815.